




# Prospect of Detecting Magnetic Fields from Strong-magnetized Binary Neutron Stars

Rundong Tang<sup>1,2</sup> , Xingyu Zhong<sup>1,2</sup>, Ye Jiang<sup>1,2</sup>, Ping Shen<sup>1,2</sup>, and Yu Wang<sup>1,3</sup>

<sup>1</sup> Shanghai Astronomical Observatory, Shanghai 200030, China; [trd@shao.ac.cn](mailto:trd@shao.ac.cn)

<sup>2</sup> School of Astronomy and Space Science, University of Chinese Academy of Sciences, Beijing 100049, China

<sup>3</sup> Guangxi Key Laboratory for Relativistic Astrophysics, School of Physical Science and Technology, Guangxi University, Nanning 530004, China

Received 2024 April 7; revised 2024 September 5; accepted 2024 September 11; published 2024 October 17

## Abstract

Binary neutron star mergers are unique sources of gravitational waves in multi-messenger astronomy. The inspiral phase of binary neutron stars can emit gravitational waves as chirp signals. The present waveform models of gravitational waves only considered the gravitational interaction. In this paper, we derive the waveform of the gravitational wave signal taking into account the presence of magnetic fields. We found that the electromagnetic interaction and radiation can introduce different frequency-dependent power laws for both the amplitude and frequency of the gravitational wave. We show from the results of the Fisher information matrix that the third-generation observation may detect magnetic dipole moments if the magnetic field is  $\sim 10^{17}$  G.

*Key words:* stars: neutron – magnetic fields – gravitational waves

## 1. Introduction

In the 20th century, the observation of the first binary pulsar PSR B1913+16 by Russell A. Hulse and Joseph H. Taylor (Hulse 1994; Taylor 1994) indicated an energy loss due to gravitational radiation. Later the GW150914 event (Abbott et al. 2016a, 2016b) marked the first direct detection of a gravitational-wave (GW) signal from the coalescing of two black holes and opened the era of GW astronomy. Then GW170817 and a gamma-ray burst announced the first direct observation of GWs from the merger of two neutron stars and subsequent electromagnetic radiation (Abbott et al. 2017; Goldstein et al. 2017). Moreover, due to the accompanying electromagnetic counterparts, this event offers an independent standard siren measurement of the Hubble constant (Hotokezaka et al. 2019). GW170817 can also afford some constraints on physics such as the nuclear coupling of light axion fields (Zhang et al. 2021) and the emitting region of the gamma-rays (Matsumoto et al. 2019). The merger of a binary neutron star system can be divided into distinct phases: an inspiral phase where the objects gradually approach, and a merger phase marked by rapid coalescence. The GW signal emitted during the inspiral phase is a source for detectors such as the Advanced LIGO/Virgo detectors (Acernese et al. 2014; Collaboration & Aasi 2015), KAGRA (Somiya 2012) (LVK) and future Einstein Telescope (ET) (Punturo et al. 2010), Taiji (Luo et al. 2020) and DECIGO (Seto et al. 2001). The Advanced LIGO/Virgo are expected to give a merger rate of binary neutron stars (BNSs) ranging from  $\sim 0.4$  to  $\sim 400$   $\text{yr}^{-1}$  (Abadie et al. 2010) and the upper limit is  $12,600$   $\text{Gpc}^{-3} \text{yr}^{-1}$  (Abbott et al. 2016c) since it has a considerable amount

distribution in our Milky Way. Lately, the study of systems that emit electromagnetic radiation when they coalesce has attracted interest due to the rich information that can be extracted from this scenario.

A neutron star gains its strong magnetic field due to the conservation of magnetic flux after the collapse (Spruit 2008). Previous observations provided that the magnetic field carried by neutron stars can reach up to  $10^{15}$  G (Ferrario & Wickramasinghe 2005). In some relativistic simulations, the magnetic fields can reach a value as strong as  $10^{18}$  G (Bocquet et al. 1995; Cardall et al. 2001). A neutron star that contains a magnetic field can be treated as a magnetic dipole. The motion of a magnetic dipole and its precession around the axis of rotation can give rise to electromagnetic radiation (Pacini 1967). Some researches show that a constant magnetic dipole moving arbitrarily can emit electromagnetic radiation (Heras 1994), since the moving magnetic dipole moment is equivalent to a current density vector and then the radiated potential can be derived by solving Maxwell equations (Heras 1994; Ioka & Taniguchi 2000; Griffiths 2011). On the other hand, when the magnetic dipole moment of a neutron star is misaligned with its spin axis, spin-down will take place due to the energy loss (Dall’Osso et al. 2011). Such neutron stars with changing magnetic dipole moments, observed as pulsars, can support rich observational effects in multi-messenger astronomy.

In the past, most research focused on GW emissions by simulating large sets of BNS systems before, during and after mergers. Many of these simulations aimed to measure the equations of state, explore the effects of magnetohydrodynamics on GWs during the process, or study the remnants

following the merger (Anderson et al. 2008; Andersson et al. 2011; Bauswein & Janka 2012; Baiotti 2019). Data analyses have been conducted to test general relativity, particularly after the detection of the GW170817 events (Abbott et al. 2019, 2019; Radice & Dai 2019; Abbott et al. 2020, 2021). The detection of GW from the inspiral phase demands accurate waveform templates owing to the weak amplitude of the wave. For the detection of BNSs, most of the present gravitational waveform models considered only the gravitational interaction containing the effects of tidal deformation and spin (Apostolatos et al. 1994; Dietrich et al. 2017). Few researches focused on the electromagnetic interaction in detail, which we will introduce and examine. Due to the presence of strong magnetic fields, both the electromagnetic dipolar interaction and energy loss can affect the evolution of orbital separation distance so that the time-evolution of orbital quadrupole moments differs from that in a purely gravitational dominant system (Vasúth et al. 2003). Energy loss of a magnetized neutron star originates not only from the GWs emission but also from the electromagnetic waves (EMWs). It is certain that the presence of magnetic dipole moments in compact objects can affect the amplitude and changing rate of the angular frequency of GWs, see Ioka & Taniguchi (2000), Henry et al. (2023). Additionally, the relativistic simulations in Bocquet et al. (1995) and Cardall et al. (2001) provides a possibility of the presence of strong magnetic fields, starting from which we deduce the frequency-domain waveform model containing the effect of magnetic dipole moments and evaluate the possibility of detection.

This article is organized as follows. In Section 2 we derive the equation of motion for two magnetized neutron stars from the circular-orbit case using the Euler–Lagrange equation. We adopt the post-Newtonian method including dipolar interaction. In Section 3 we calculate the total energy loss rate contributed by both gravitational radiation and electromagnetic radiation averaged over a period in the adiabatic approximation. We use this result to compute the time derivative of orbital radius and further derive the waveform governed by gravitational and electromagnetic interaction by performing the Fourier transform and stationary phase approximation in Section 4. We compare the waveform containing the influence of magnetic field with that predicted for a system dominated by pure gravity, using matched-filtering techniques for LIGO and ET in Section 5. In addition, we report in this section the results of evaluating the parameter estimation obtained from the Fisher information matrix.

## 2. Equation of Motion for a Bound Binary System

Throughout this paper, we choose Gaussian units such that  $\frac{\mu_0}{4\pi} = \frac{1}{4\pi\epsilon_0} = 1$  and keep gravitational constant  $G$  and the speed of light  $c$  within the expressions. For a binary system formed with a long initial separation, it spends most of its lifetime in the inspiral phase (Maggiore 2007; Liu et al. 2020; Chu et al. 2022)

during which the lowest-order post-Newtonian approximation is employed to describe it. Thus we consider the Keplerian orbits of two magnetized neutron stars with masses  $m_1$  and  $m_2$  and magnetic dipole moments  $\mathbf{d}_1$  and  $\mathbf{d}_2$ , respectively. For simplicity, we assume that the magnetic dipole moments of these two neutron stars are aligned with their respective spin axes and with the angular momenta of orbits. Note that we considered neither the higher order post-Newtonian corrections nor the full general relativity since in the long-distance inspiral phase the interactions between the EM and gravitational fields enter the 2.5 post-Newtonian order ( $\sim \mathcal{O}(c^{-5})$ ), see Henry et al. (2024), which is negligible. In addition, the internal currents that generate the magnetic field of the primary are not distorted significantly by the external field of the secondary and vice-versa since they are well-separated (Bourgoin et al. 2022). Furthermore, the contribution of electromagnetic fields to spacetime is much less than the masses and can be neglected (Ioka & Taniguchi 2000).

It is necessary to introduce the relationship between the magnetic dipole moment and the surface magnetic field  $B$  at pole:  $d \equiv |\mathbf{d}| = \frac{1}{2}R_N^3 B$ , where  $R_N$  is the radius of a neutron star, and we set the same radius for the two neutron stars throughout this paper. Moreover, we neglect the influence of spin on the orbital motions. Due to electromagnetic interaction, the orbits will differ from those of a binary system dominated solely by gravity.

Given a dipole  $\mathbf{d}_2$  immersed in the field generated by a dipole  $\mathbf{d}_1$ , the interaction potential energy is, according to field theory (Landau & Lifshitz 1975):

$$U_D = \frac{\mathbf{d}_1 \cdot \mathbf{d}_2 - 3(\mathbf{d}_1 \cdot \mathbf{R}_u)(\mathbf{d}_2 \cdot \mathbf{R}_u)}{R^3}, \quad (1)$$

here we have defined  $R = |\mathbf{R}|$ ,  $\mathbf{R} = \mathbf{r}_1 - \mathbf{r}_2$  and  $\mathbf{R}_u = \mathbf{R}/R$ . In our case, this expression is simplified as

$$U_D = \frac{d_1 d_2}{R^3}, \quad (2)$$

The Lagrangian for the bound system is given by

$$L = \frac{1}{2}m_1\dot{\mathbf{r}}_1^2 + \frac{1}{2}m_2\dot{\mathbf{r}}_2^2 + \frac{Gm_1m_2}{R} - \frac{d_1 d_2}{R^3}. \quad (3)$$

The above dot denotes the derivation with respect to time  $t$ . It is convenient to choose the center of mass as the origin of coordinates, i.e.,

$$\mathbf{r}_{\text{CM}} = \sum_{i=1}^2 \frac{m_i \mathbf{r}_i}{M} = (0, 0), \quad (4)$$

where,  $M = m_1 + m_2$  is the total mass of the system. Therefore,  $\mathbf{r}_1 = m_2 \mathbf{R}/M$  and  $\mathbf{r}_2 = -m_1 \mathbf{R}/M$ . By introducing the reduced mass  $\mu = m_1 m_2 / M$  and transforming to polar coordinates  $(r, \varphi)$ , we can rewrite the Lagrangian as

$$L = \frac{1}{2}\mu\dot{R}^2 + \frac{1}{2}\mu R^2\dot{\varphi}^2 + \frac{G\mu M}{R} - \frac{d_1 d_2}{R^3} = T - U. \quad (5)$$

According to Equation (5), we find that the respective kinetic and potential energies are:

$$T = \frac{1}{2}\mu\dot{R}^2 + \frac{1}{2}\mu R^2\dot{\varphi}^2, \quad (6)$$

$$U = -\frac{G\mu M}{R} + \frac{d_1 d_2}{R^3}. \quad (7)$$

It is clear that the system has 2 degrees of freedom and the orbital motion of the system takes place in a two-dimensional space. We can express the Euler–Lagrange equation in terms of the  $\varphi$  dimension as:

$$\frac{d}{dt}\left(\frac{\partial L}{\partial \dot{\varphi}}\right) - \frac{\partial L}{\partial \varphi} = \frac{d}{dt}(\mu R^2 \dot{\varphi}) = 0. \quad (8)$$

Furthermore, the canonical momentum  $P_\varphi$  is given by

$$P_\varphi = \frac{\partial L}{\partial \dot{\varphi}} = \mu R^2 \dot{\varphi}. \quad (9)$$

As a result, the canonical momentum  $P_\varphi$ , commonly referred to as the orbital angular momentum  $l$ , is conserved throughout the process. This gives the relationship between angular velocity and angular momentum:

$$\dot{\varphi} = \frac{l}{\mu R^2}. \quad (10)$$

Subsequently, if we examine the Euler–Lagrange equation for  $R$ , we obtain:

$$\frac{d}{dt}\left(\frac{\partial L}{\partial \dot{R}}\right) - \frac{\partial L}{\partial R} = \mu\ddot{R} - \left(\frac{l^2}{\mu R^3} - \frac{G\mu M}{R^2} + \frac{3d_1 d_2}{R^4}\right) = 0. \quad (11)$$

Multiply by a factor  $\dot{R}$  on both sides of Equation (11) we find

$$\frac{d}{dt}\left(\frac{1}{2}\mu\dot{R}^2 + \frac{l^2}{2\mu R^2} - \frac{G\mu M}{R} + \frac{d_1 d_2}{R^3}\right) = 0, \quad (12)$$

and so the total energy of this system

$$E = \frac{1}{2}\mu\dot{R}^2 + \frac{l^2}{2\mu R^2} - \frac{G\mu M}{R} + \frac{d_1 d_2}{R^3} \quad (13)$$

is conserved, as expected. Under the circular condition, both the radial velocity and acceleration vanish, leading to a simplified equation of motion:

$$\mu\omega_s^2 R = \frac{G\mu M}{R^2} - \frac{3d_1 d_2}{R^4}, \quad (14)$$

where we have defined  $\dot{\varphi} \equiv \omega_s$ , obviously it is a constant.

### 3. Evolution of Orbital Radius

According to the Virial theorem, for an  $N$ -body system bounded by a potential, if the potential energy  $U$  is the sum of power functions of  $r$ :  $U = \sum a_n r^n$ , the relationship between the

average total kinematic energy and potential energy is

$$\langle T \rangle = \frac{1}{2} \langle \nabla U \cdot \mathbf{r} \rangle = \frac{1}{2} \sum_n a_n n r^n, \quad (15)$$

where  $n < -1$  for BNS system such that the potential reaches zero asymptotically at infinity. Thus the kinematic energy in our case can be written as

$$T = \frac{1}{2} \left( \frac{G\mu M}{R} - \frac{3d_1 d_2}{R^3} \right), \quad (16)$$

so the total energy has the form:

$$E = -\frac{G\mu M}{2R} - \frac{d_1 d_2}{2R^3} = -\frac{G\mu M}{2R} \left( 1 + \frac{d_1 d_2}{G\mu M} \frac{1}{R^2} \right). \quad (17)$$

#### 3.1. Electromagnetic Radiation

Due to the presence of both gravitational and electromagnetic radiation, the conservation of total energy is no longer maintained. We will start by investigating the energy emission resulting from electromagnetic radiation. We also point out that the magnetic reconnection will contribute to energy loss and bring more phenomena. However, it is very complicated and we will consider it in future research. As the neutron star is moving, it is necessary to consider the transformation of electromagnetic fields in two reference frames. Denoting the rest frame of the neutron star by  $S'$  and the observer frame by  $S$ , the magnetic dipole moment  $\mathbf{d}'$  in  $S'$  is static. When  $S'$  moves with arbitrary velocity  $\mathbf{v}$ , it will induce an electric dipole moment  $\mathbf{d}_e$  according to the Lorentz transformation of the 4-potential  $A_\mu$ . In the low-velocity limit, the electric dipole moment can be expressed as, in the frame  $S$  (Griffiths 2005),

$$\mathbf{d}_e = \frac{\mathbf{v} \times \mathbf{d}'}{c^2}. \quad (18)$$

On the other hand, the radiated field  $\mathbf{B}_R$  at field point  $\mathbf{r}$  of a magnetic dipole in arbitrary motion  $\mathbf{s}(t')$  is calculated by Heras (Heras 1994):

$$\begin{aligned} \mathbf{B}_R = & \frac{3\mathbf{D}_u \times (\mathbf{D}_u \times \mathbf{d}' - c\mathbf{d}_e)(\mathbf{D}_u \cdot \mathbf{a})^2}{DK^5 c^4} \\ & + \frac{3\mathbf{D}_u \times (\mathbf{D}_u \times \mathbf{d}' - c\dot{\mathbf{d}}_e)(\mathbf{D}_u \cdot \mathbf{a})}{DK^4 c^3} \\ & + \frac{\mathbf{D}_u \times (\mathbf{D}_u \times \mathbf{d}' - c\mathbf{d}_e)(\mathbf{D}_u \cdot \dot{\mathbf{a}})}{DK^4 c^3} \\ & + \frac{\mathbf{D}_u \times (\mathbf{D}_u \times \ddot{\mathbf{d}}' - c\dot{\mathbf{d}}_e)}{DK^3 c^2}, \end{aligned} \quad (19)$$

where  $D = |\mathbf{r} - \mathbf{s}(t')|$ ,  $\mathbf{D}_u = (\mathbf{r} - \mathbf{s}(t'))/D$ ,  $K = 1 - \mathbf{v} \cdot \mathbf{D}_u/c$  and  $\mathbf{a} = \dot{\mathbf{v}}$ . This expression is complicated. Under the low-velocity limit and if we consider the source is small in comparison with the distance i.e.,  $|\mathbf{s}(t')|/D < 1$ , the

calculation can be performed up to the leading order of  $v/c$  and  $|\mathbf{s}(t')|/D$ , following Ioka & Taniguchi (2000):

$$\mathbf{B}_R = \frac{1}{Dc^3}(\mathbf{D}_u \cdot \mathbf{d}')[(\mathbf{D}_u \cdot \dot{\mathbf{a}})\mathbf{D}_u - \dot{\mathbf{a}}]. \quad (20)$$

Then we can calculate the total power of electromagnetic wave by integrating over the solid angle (Landau & Lifshitz 1975):

$$P_{\text{EM}} = \int \frac{dP_{\text{EM}}}{d\Omega} d\Omega = \int \frac{cB_R^2 D^2}{4\pi} d\Omega. \quad (21)$$

The only well-defined energy emission power is given by the time average over one period of the wave:

$$\bar{P}_{\text{EM}} = \frac{1}{T} \int_0^T dt P_{\text{EM}}. \quad (22)$$

So the energy emission power averaged over a period is given by

$$\left\langle \frac{dE_{\text{EM}}}{dt} \right\rangle = -\bar{P}_{\text{EM}} = \frac{4d^2 R^2 \omega_s^6}{15c^5}, \quad (23)$$

where  $d$  is the modulus of the effective magnetic dipole moment  $\mathbf{d} = (m_2 \mathbf{d}_1 - m_1 \mathbf{d}_2)/M$ .

However, the Lorentz boost of the inspiraling neutron star is different at two different times due to the changing direction of velocity. The total Lorentz transformation can be treated as a Lorentz boost plus a pure rotation (Jackson 2021). This will lead to an additional evolution called Thomas precession. We considered two different cases for the evolution of magnetic dipole moments due to the Thomas precession.

Due to the Lorentz transformation, the Lorentz boost is different between two inertial reference frames with different directions of motion. In the circular orbital, the Lorentz boost is different since the velocity of the neutron star changes with time. Then the neutron star will obtain an additional angular velocity due to the precession (Jackson 2021):

$$\boldsymbol{\omega}_T = \frac{\gamma^2}{\gamma + 1} \frac{\mathbf{a} \times \mathbf{v}}{c^2}, \quad (24)$$

where  $\mathbf{a}$ ,  $\mathbf{v}$  are the acceleration and velocity of a neutron star respectively. Then an observer in the rest frame  $S$  will see that a vector  $\mathbf{G}$  in the frame of circular motion  $S'$  gains an additional time evolution:

$$\dot{\mathbf{G}} = \boldsymbol{\omega}_T \times \mathbf{G}. \quad (25)$$

First for circular orbits with two dipoles both aligned with the orbital angular momentum. The acceleration and velocity are perpendicular to each other and both in the orbital plane, thus the cross-product points to the normal of the orbital plane. We set the direction of angular momentum to be the  $z$ -axis and thus the angular velocity vector is along the  $z$ -axis and parallel to the two dipoles. This gives the zero changing rate of dipoles:

$$\dot{\mathbf{d}} = \boldsymbol{\omega}_T \times \mathbf{d} = 0, \quad (26)$$

and so the second order derivative is:

$$\ddot{\mathbf{d}} = 0, \quad (27)$$

thus there is no dipole radiation due to the Thomas precession.

Second, we consider that one of the dipoles is not parallel to the angular momentum, e.g.,  $\mathbf{d}_2$ . Suppose that there is an angle of inclination as  $\epsilon$ , that is,  $\mathbf{d}_2 \cdot \mathbf{e}_z = d_2 \cos \epsilon$ . Note that since the total angular momentum of the binary neutron star is conserved, the orbital angular momentum will change with time, so the motion is generally three-dimensional. However, we can still require that the orbit is circular just for a rough estimation of the magnitude of the radiation power.

Due to the Thomas precession, the changing rate of  $\mathbf{d}_2$  is given as:

$$\dot{\mathbf{d}}_2 = \boldsymbol{\omega}_T \times \mathbf{d}_2 = \frac{\gamma^2}{\gamma + 1} \frac{\mathbf{a}_2 \times \mathbf{v}_2}{c^2} \times \mathbf{d}_2. \quad (28)$$

Then we derivative the rate with respect to time, we obtain:

$$\begin{aligned} \ddot{\mathbf{d}}_2 &= \frac{\gamma^2}{c^2(\gamma + 1)} [(\dot{\mathbf{a}}_2 \times \mathbf{v}_2) \times \mathbf{d}_2 + (\mathbf{a}_2 \times \dot{\mathbf{v}}_2) \\ &\quad \times \mathbf{d}_2 + (\mathbf{a}_2 \times \mathbf{v}_2) \times \dot{\mathbf{d}}_2]. \end{aligned} \quad (29)$$

Note that in the assumption of circular orbits we have  $\dot{\mathbf{a}}_2 \times \mathbf{v}_2 = 0$ ,  $\mathbf{a}_2 \times \dot{\mathbf{v}}_2 = 0$  and  $\mathbf{a}_2 \times \mathbf{v}_2 \propto \omega_s^3$ . Thus the second derivative reads:

$$\begin{aligned} \ddot{\mathbf{d}}_2 &= \frac{\gamma^2}{c^2(\gamma + 1)} (\mathbf{a}_2 \times \mathbf{v}_2) \times \left[ \frac{\gamma^2}{\gamma + 1} \frac{\mathbf{a}_2 \times \mathbf{v}_2}{c^2} \times \mathbf{d}_2 \right] \\ &= \left[ \frac{\gamma^2}{c^2(\gamma + 1)} \right]^2 [(\mathbf{a}_2 \times \mathbf{v}_2)(\mathbf{a}_2 \times \mathbf{v}_2) \cdot \mathbf{d}_2 - \mathbf{d}_2 |\mathbf{a}_2 \times \mathbf{v}_2|^2] \\ &\propto \frac{\omega_s^6}{c^4} \end{aligned} \quad (30)$$

According to dipole radiation, the power of such a changing magnetic dipole moment is roughly:

$$P_T \propto |\ddot{\mathbf{d}}_2|^2 \propto \frac{\omega_s^{12}}{c^8}. \quad (31)$$

Thus the magnitude of radiation power is much less than Equation (23). In summary, from the estimate of magnitude, the additional radiation power from Thomas precession can be neglected.

### 3.2. Gravitational Radiation

To continue, we need to calculate the energy emission from gravitational radiation. Following Maggiore (2007), the total radiated power in the quadrupole approximation integrated over all the directions is (we have employed the Einstein

summation convention)

$$P_{\text{GW}} = \frac{G}{5c^5} \langle \ddot{M}_{ij} \ddot{M}_{ij} - \frac{1}{3} (\ddot{M}_{kk})^2 \rangle, \quad (32)$$

with the mass quadrupole moment in the equatorial plane:

$$M_{ij} = \mu x^i x^j. \quad (33)$$

We are working on the case of a circular orbit and a sufficiently slow rate of emission of GW, so the radius of the binary and the time derivative of  $\varphi$  remain constant instantaneously. According to the relation between Cartesian coordinates and polar coordinates, we finally derive the specific expressions of non-zero components of mass quadrupole moments:

$$\begin{aligned} \ddot{M}_{11} &= \frac{4(GM)^{3/2} \mu^{5/2}}{R^{7/2}} \left( 1 - \frac{3d_1 d_2}{G\mu M} \frac{1}{R^2} \right)^{3/2} \sin 2\varphi, \\ \ddot{M}_{12} &= \ddot{M}_{21} = \frac{-4(GM)^{3/2} \mu^{5/2}}{R^{7/2}} \left( 1 - \frac{3d_1 d_2}{G\mu M} \frac{1}{R^2} \right)^{3/2} \cos 2\varphi, \\ \ddot{M}_{22} &= \frac{-4(GM)^{3/2} \mu^{5/2}}{R^{7/2}} \left( 1 - \frac{3d_1 d_2}{G\mu M} \frac{1}{R^2} \right)^{3/2} \sin 2\varphi. \end{aligned} \quad (34)$$

Note that the emission power of GWs averaged over one period is the same as the instantaneous power:

$$\bar{P}_{\text{GW}} = P_{\text{GW}}. \quad (35)$$

Therefore, the energy emission power of GWs averaged over one period is

$$\left\langle \frac{dE_{\text{GW}}}{dt} \right\rangle = -\bar{P}_{\text{GW}} = \frac{32G\mu^2 R^4 \omega_s^6}{5c^5}. \quad (36)$$

and finally the rate of total energy emission is

$$\left\langle \frac{dE}{dt} \right\rangle = \left\langle \frac{dE_{\text{EM}}}{dt} \right\rangle + \left\langle \frac{dE_{\text{GW}}}{dt} \right\rangle. \quad (37)$$

### 3.3. Evolution of Orbital Separation

Due to the loss of energy, the separation distance of the binary is reduced and the two neutron stars merge. We neglect higher-order post-Newtonian or general relativistic corrections to the flux since they start at  $\sim \mathcal{O}(c^{-9})$  (Henry et al. 2024). By performing time derivatives on both sides of Equation (17) gives the relation between the time evolution of  $R$  and the energy loss rate. Throughout this paper, we regard the electromagnetic interaction as a perturbation of orbits, i.e.,  $\frac{d_1 d_2}{Gm_1 m_2} \frac{1}{R^2} < 1$ . Furthermore, from Equation (14) we have

$$\omega_s^2 = \frac{GM}{R^3} - \frac{3d_1 d_2}{\mu R^5} = \frac{GM}{R^3} \left( 1 - \frac{3d_1 d_2}{G\mu M} \frac{1}{R^2} \right), \quad (38)$$

then we derive  $\dot{R}$  to the first order of  $d_1 d_2 / (G\mu M R^2)$ :

$$\frac{dR}{dt} = -\frac{64G^3 \mu M^2}{5c^5 R^3} \left( 1 - \frac{12d_1 d_2}{G\mu M} \frac{1}{R^2} + \frac{d^2}{24G\mu^2} \frac{1}{R^2} \right). \quad (39)$$

To continue our analysis, it is convenient to introduce dimensionless expressions. It is needed to introduce the characteristic radius:

$$R_*^3 = \left( \frac{2GM}{c^2} \right)^2 \left( \frac{G\mu}{c^2} \right). \quad (40)$$

We can therefore rewrite quantities such as  $t$ ,  $R$ ,  $M$  as a dimensionless expression  $\hat{t} = ct/R_*$ ,  $\hat{R} = R/R_*$ ,  $\hat{\mathcal{M}} = G\mathcal{M}/(c^2 R_*)$ , where  $\mathcal{M}$  represents any mass term such as the total mass and the reduced mass and the hat symbol above denotes the dimensionless expression. Note that  $d_i/(\sqrt{G}m_i)$  ( $i = 1, 2$ ) has the dimension of  $[R]$ , so the dimensionless expression is  $\hat{d}_i = d_i/(\sqrt{G}m_i R_*)$ . Then Equation (39) can be rewritten as

$$\begin{aligned} \frac{d\hat{R}}{d\hat{t}} &= -\frac{16}{5} \frac{1}{\hat{R}^3} \left[ 1 - \left( 12\hat{d}_1 \hat{d}_2 - \frac{\hat{d}^2}{24} \right) \frac{1}{\hat{R}^2} \right] \\ &= -\frac{\beta}{\hat{R}^3} - \frac{\alpha}{\hat{R}^5}, \end{aligned} \quad (41)$$

where we have defined  $\beta = \frac{16}{5}$ ,  $\alpha = \frac{16}{5} \left( \frac{\hat{d}^2}{24} - 12\hat{d}_1 \hat{d}_2 \right)$ . We can integrate the differential equation as

$$-\int_{\hat{R}_0}^{\hat{R}} \frac{\hat{R}^5}{\gamma \hat{R}^2 + 1} d\hat{R} = \alpha \hat{t}, \quad (42)$$

where  $\gamma = \beta/\alpha$  and we set the initial time to be 0. This gives the solution:

$$f(\hat{R}_0) - f(\hat{R}) = \alpha \hat{t}, \quad (43)$$

$$f(\hat{R}) = \frac{\ln(1 + \gamma \hat{R}^2)}{2\gamma^3} - \frac{\hat{R}^2}{2\gamma^2} + \frac{\hat{R}^4}{4\gamma}. \quad (44)$$

According to an estimation of the magnitude, the logarithm is much less than the power parts in the expression, so we neglect the contribution of the first term in the right hand of Equation (44), thus we approximately have

$$f(\hat{R}) \simeq -\frac{\hat{R}^2}{2\gamma^2} + \frac{\hat{R}^4}{4\gamma}. \quad (45)$$

In order to solve Equation (43), we need to define the time to coalescence  $\hat{\tau}$  through  $\hat{\tau} + \hat{t} = \hat{t}_0 = \hat{\tau}_0$  and  $\hat{t}_0$  is the time when the two neutron stars coalesce. So Equation (43) becomes (Christiansen et al. 2021):

$$f(\hat{R}_0) - f(\hat{R}) = \alpha(\hat{\tau}_0 - \hat{\tau}). \quad (46)$$



From this equation we can get the relationship between  $\hat{R}$  and  $\hat{\tau}$ :

$$\hat{R} = \sqrt{\frac{1}{\gamma}(1 + \sqrt{1 + 4\alpha\gamma^3\hat{\tau}})}. \quad (47)$$

In our analysis we considered the assumption that  $\gamma \gg 1$ . Actually, the terms of  $\hat{d}_i$  in  $\alpha$  is much less than the unit even though we choose a large value of  $B$ , which can be seen by substituting some actual values into the dimensionless expressions. Finally, we have the approximate solution to the first order of  $1/\gamma$ :

$$\hat{R} = (4\beta\hat{\tau})^{1/4} \left[ 1 + \frac{1}{2\gamma}(4\beta\hat{\tau})^{-1/2} \right]. \quad (48)$$

By inserting  $\hat{R}$  into Equation (38) and expanding to the leading order we get (notice the magnitude  $\hat{d}_1\hat{d}_2 \sim 1/\gamma$ ):

$$\begin{aligned} \hat{\omega}_s &= 2^{-3/4} \hat{M}_c^{-5/8} (4\beta\hat{\tau})^{-3/8} \\ &\times \left[ 1 - \left( \frac{3}{2} \hat{d}_1 \hat{d}_2 + \frac{3}{4\gamma} \right) (4\beta\hat{\tau})^{-1/2} \right]. \end{aligned} \quad (49)$$

here we set  $\hat{\omega}_s = R_* \omega_s / c$  and define the chirp mass as  $M_c = \mu^{3/5} M^{2/5}$  together with its dimensionless expression  $\hat{M}_c \equiv GM_c / (c^2 R_*)$ .

#### 4. Waveform of Gravitational Waves

In the theoretical analysis of waveform, we calculate the waveform in harmonic coordinates, thus there are only two independent components: the plus polarization

$$h_+(\hat{t}) = \frac{4\hat{\mu}\hat{\omega}_s^2 \hat{R}^2}{\hat{D}} \left( \frac{1 + \cos^2 \iota}{2} \right) \cos \Phi \quad (50)$$

and the cross polarization

$$h_\times(\hat{t}) = \frac{4\hat{\mu}\hat{\omega}_s^2 \hat{R}^2}{\hat{D}} \cos \iota \sin \Phi, \quad (51)$$

here  $\iota$  is the angle between the orbital angular momentum and the line of sight of the observer and  $\hat{D}$  is the dimensionless luminosity distance from the binary to the observer. We select  $\iota = \pi/2$  so that the GW observed has only plus polarization:

$$h_+(\hat{t}) = \frac{2\hat{\mu}\hat{\omega}_s^2 \hat{R}^2}{\hat{D}} \cos \Phi, \quad (52)$$

with the phase defined as:

$$\Phi(\hat{t}) = 2 \int_{\hat{t}_0}^{\hat{t}} \hat{\omega}_s(\hat{t}') d\hat{t}' = \int_{\hat{t}_0}^{\hat{t}} \hat{\omega}_{GW}(\hat{t}') d\hat{t}' \quad (53)$$

where  $\omega_{GW} = 2\omega_s$  is known as the chirping frequency. From Equation (49) we can see that  $\omega_{GW}$  increases as the binary approaches the coalescence, i.e.,  $\hat{\tau}$  decreases. Substituting

Equations (48) and (49) into Equation (52), we obtain:

$$h_+(\hat{t}) = A(\hat{\tau}) \cos \Phi, \quad (54)$$

with

$$\begin{aligned} A(\hat{\tau}) &\simeq \frac{\sqrt{2}}{\hat{D}} \hat{M}_c^{5/4} (4\beta\hat{\tau})^{-1/4} \\ &\times \left[ 1 - \left( \frac{1}{2\gamma} + 3\hat{d}_1\hat{d}_2 \right) (4\beta\hat{\tau})^{-1/2} \right]. \end{aligned} \quad (55)$$

To observe the effects of magnetic dipole moments, we plotted the waveforms of magnetized and non-magnetized neutron stars in Figure 1. Note that we set the magnetic field to be of order  $\sim 10^{17}$ , under the relativistic simulation results of Cardall et al. (2001). The equations show that the magnetic dipole moments contribute additional  $\hat{\tau}$  terms to both the frequency  $\omega_{GW}(\hat{\tau})$  and amplitude  $A(\hat{\tau})$  of the wave. The additional frequency terms induce a considerable phase shift compared with the case where there are no magnetic dipole moments. Also, both the amplitude and frequency increase gradually as coalescence is approached. So the property is referred to as “chirp.”

Each detector is sensitive to signals within a specific frequency range, which varies depending on the instrument. For instance, the LIGO operates within 10 Hz–1000 Hz and  $10^{-4}$  Hz– $10^{-1}$  Hz for LISA and Taiji (LISA Study Team 1997; Collaboration & Aasi 2015; Luo et al. 2020). In order to know the frequency distribution of a signal, it is needed to take Fourier transform and rewrite the signal waveform in the frequency domain. The expression is:

$$\tilde{h}_+(f) = \int_{-\infty}^{+\infty} dt h_+(t_r) e^{i2\pi f t_r}. \quad (56)$$

Note that the GW propagates at the speed of light  $c$ , when a wave front is emitted from a source, it takes some time to reach the observer, so the integrand must be evaluated at the retarded time  $t_r = t - D/c$ . Taking into account that the differential of the retarded time is  $dt_r = dt$  and that  $\cos \Phi = \frac{1}{2}(e^{i\Phi} + e^{-i\Phi})$ , we can rewrite the expression as:

$$\begin{aligned} \tilde{h}_+(f) &= \frac{1}{2} e^{i2\pi f D/c} \int_{-\infty}^{+\infty} dt_r A(t_r) \\ &\times (e^{i\Phi(t_r)} + e^{-i\Phi(t_r)}) e^{i2\pi f t_r}. \end{aligned} \quad (57)$$

Following Maggiore (2007), we use the stationary phase approximation, where only the term  $e^{i(-\Phi + 2\pi f t)}$  has stationary point, while the term  $e^{i(\Phi + 2\pi f t)}$  oscillates fast that will be integrated to a negligibly small value. Thus the expression reduces to

$$\tilde{h}_+(f) \simeq \frac{1}{2} e^{i2\pi f D/c} \int_{-\infty}^{+\infty} dt_r A(t_r) e^{i[2\pi f t_r - \Phi(t_r)]}. \quad (58)$$

At the stationary point  $t_*$  we have  $2\pi f = \dot{\Phi}(t_*) \equiv \omega_{GW}$ . This indicates that the largest contribution to Fourier components is

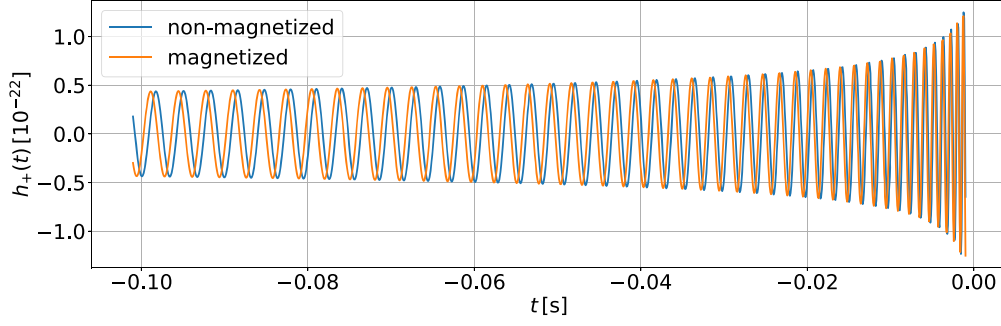


**Figure 1.** Time-domain waveform of  $h_+(t)$ : The reference point for time is set at the coalescence time  $t_c$ . We have selected  $m_1 = m_2 = 1.55 M_\odot$  so that the chirp mass is  $M_c \simeq 1.39 M_\odot$ . We set  $R_N = 13.8$  km for the two neutron stars and  $D = 100$  Mpc. For the magnetized neutron stars, we choose the surface magnetic field as  $8 \times 10^{17}$  G.

obtained for the value  $t$  such that  $\omega_{\text{GW}}$  is equal to  $2\pi f$ . Taking into account that  $A(t_r)$  varies much more slowly compared to phase, we expand the expression around the point  $t_*$  to the second order of  $(t - t_*)$  and ultimately obtain:

$$\tilde{h}_+(f) = \frac{1}{2} e^{i\Psi_+} A(t_*) \left( \frac{2}{\ddot{\Phi}(t_*)} \right)^{1/2}, \quad (59)$$

where  $\Psi_+(t_*) = 2\pi f(t_* + D/c) - \Phi(t_*) - \pi/4$ . From Equation (49) we can immediately get, keeping it in mind that  $\omega_{\text{GW}}$  is twice the angular velocity,

$$\begin{aligned} \Phi(\hat{\tau}) = \Phi(\hat{\tau}_0) - 2^{1/4} \hat{M}_c^{-5/8} & \left[ \frac{8}{5} (4\beta)^{-3/8} \hat{\tau}^{5/8} \right. \\ & \left. - \left( 12\hat{d}_1\hat{d}_2 + \frac{6}{\gamma} \right) (4\beta)^{-7/8} \hat{\tau}^{1/8} \right]. \end{aligned} \quad (60)$$

To get the relation between  $t_*$  and  $f$ , or equivalently between  $\tau_*$  and  $f$  we need to solve the equation:

$$\dot{\Phi}(\hat{\tau}_*) = \frac{d}{dt} \Phi(\hat{\tau})|_{\hat{\tau}=\hat{\tau}_*} = -\frac{d}{d\tau} \Phi(\hat{\tau})|_{\hat{\tau}=\hat{\tau}_*} = 2\pi f, \quad (61)$$

thus we derive the frequency:

$$\begin{aligned} \hat{f} = \frac{2^{-3/4}}{\pi} \hat{M}_c^{-5/8} (4\beta\hat{\tau}_*)^{-3/8} \\ \times \left[ 1 - \left( \frac{3}{2} \hat{d}_1\hat{d}_2 + \frac{3}{4\gamma} \right) (4\beta\hat{\tau}_*)^{-1/2} \right]. \end{aligned} \quad (62)$$

Since the electromagnetic interaction is much weaker than gravity, we neglect the contribution of magnetic dipole and obtain the relation:

$$\hat{\tau}_* \simeq \frac{1}{16\beta} \hat{M}_c^{-5/3} (\pi\hat{f})^{-8/3}. \quad (63)$$

Substituting Equation (63) into the expressions of  $A(\hat{\tau}_*)$  and  $\ddot{\Phi}(\hat{\tau}_*)$  in Equation (59) and restoring  $G$ ,  $c$  we finally obtained

the full expression in frequency domain for further analysis:

$$\begin{aligned} \tilde{h}_+(f) = e^{i\Psi_+} \frac{c}{D} \left( \frac{5}{96} \right)^{1/2} \\ \times \left[ \pi^{-2/3} \left( \frac{GM_c}{c^3} \right)^{5/6} f^{-7/6} - \frac{\pi^{2/3}}{2} c^{-2} \left( \frac{GM_c}{c^3} \right)^{1/6} \right. \\ \left. \times \left( \frac{\mu}{M} \right)^{2/5} \left( \frac{d^2}{24G\mu^2} - \frac{6d_1d_2}{Gm_1m_2} \right) f^{1/6} \right], \end{aligned} \quad (64)$$

where the phase is given by

$$\begin{aligned} \Psi_+(f) = \Psi_0 + 2\pi f \left( \frac{D}{c} + t_0 \right) \\ + \frac{3}{128} \pi^{-5/3} \left( \frac{GM_c}{c^3} \right)^{-5/3} f^{-5/3} - \frac{15}{64} \pi^{-1/3} c^{-2} \\ \times \left( \frac{GM_c}{c^3} \right)^{-7/3} \left( \frac{\mu}{M} \right)^{2/5} \left( \frac{d^2}{24G\mu^2} - \frac{10d_1d_2}{Gm_1m_2} \right) f^{-1/3}. \end{aligned} \quad (65)$$

All the variables associated with a constant phase have been grouped together into  $\Psi_0$ . Moreover, since  $h_+(t)$  is already dimensionless, the frequency-domain expression  $\tilde{h}_+(f)$  carries the dimension of  $[T]^{-1}$ . Clearly, the alteration of magnetic dipole moments in waveform (64) introduces different dependencies on frequency in both amplitude and phase, ultimately reducing to the scenario where only gravity dominants, namely initial waveform:

$$\begin{aligned} \tilde{h}_{i,+}(f) = e^{i\Psi_{i,+}} \frac{c}{D} \left( \frac{5}{96} \right)^{1/2} \\ \times \pi^{-2/3} \left( \frac{GM_c}{c^3} \right)^{5/6} f^{-7/6}, \end{aligned} \quad (66)$$

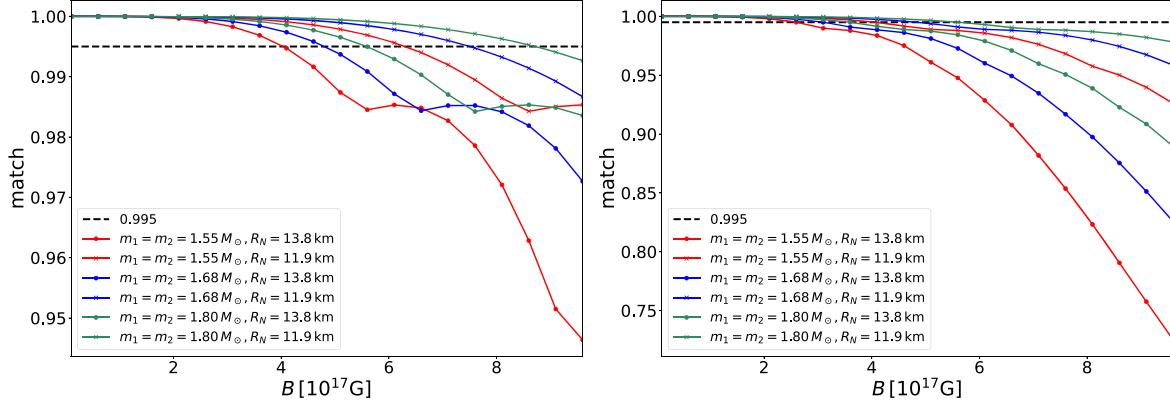


**Figure 2.** Matches between the waveforms with magnetized and non-magnetized neutron stars. We set different surface magnetic fields for magnetized neutron stars. Different colors refer to different masses. The black dashed line denotes the critical value of match below which the detector is expected to well distinguish two waveforms. The left panel shows the values of the match for the LIGO detector and the right panel is for ET.

with phase

$$\Psi_{i,+}(f) = \Psi_{i,0} + 2\pi f \left( \frac{D}{c} + t_0 \right) + \frac{3}{128} \pi^{-5/3} \left( \frac{GM_c}{c^3} \right)^{-5/3} f^{-5/3}. \quad (67)$$

## 5. Data Analysis

Using the waveform, we can analyze the dependence of  $\tilde{h}_+(f)$  on the physical properties of neutron stars, especially the surface magnetic field  $B$ . We also estimated how accurately the parameters will be identified in future observations. In our analysis, we choose  $d_2 = d_1/2000$  where the approximation  $\gamma \gg 1$  is satisfied.

### 5.1. Matched Filtering

The matched filtering technique is used here to search for deviation between two waveforms. We introduce the inner product between two time series  $a(t)$  and  $b(t)$  (Lindblom et al. 2008):

$$(a|b) = 4 \operatorname{Re} \int_0^{+\infty} \frac{\tilde{a}(f) \tilde{b}^*(f)}{S_n(f)} df. \quad (68)$$

The tilde symbols stand for the Fourier transform and the star denotes the complex conjugation. The quantity  $S_n(f)$  is the power spectral density (PSD) of noise for a particular detector.

We use this method to quantify the differences between our modified waveform and initial waveform from which we learn the influence of magnetic dipole. We calculate the maximized fitting factor or match between two signals to quantify the similarity between them:

$$\text{match} = \max_{t_s, \phi_s} \frac{(a(t)|b(t+t_s)e^{i\phi_s})}{\sqrt{(a|a)(b|b)}}, \quad (69)$$

where the maximization is taken after some proper shift of  $t_s$  and  $\phi_s$ . As the post-Newtonian approximation is applicable in the long-distance condition, the computation must be cut off

well before one neutron star reaches the innermost stable circular orbits.

Using the relationship between magnetic dipole moment and the surface magnetic field, we compute different matches for different surface magnetic fields in the frequency domain. To provide a comparison, we calculated the match for two GW detectors and illustrated the result of matched-filtering using fixed masses and radii for the neutron stars. As depicted in the figures of values of the match, we computed in the 10 Hz–1000 Hz frequency range in Figures 2 and 3 for the range  $10^{-4}$  Hz–0.1 Hz (the frequency ranges are considered to cover the detectabilities of Taiji and DECIGO (Seto et al. 2001; Luo et al. 2020.)) Note that  $R_N$  has the same value for two neutron stars. We observe that the match diminishes as masses decrease. This results from that GWs are generated due to the changing mass quadrupole moments. As we choose the electromagnetic interaction to be a perturbation of this orbital behavior, the deviation between two waveforms remains small for magnetic fields  $< 10^{17}$  G. Note that in our research we mainly focus on whether the frequency domain waveform can include the information of magnetic dipole moments in the lowest-order Newtonian approximation. We choose the magnetic fields to be  $8 \times 10^{17}$  G just as a special case or an upper limit, not for the results of current observations. Since the tidal deformation contributes fifth-order post-Newtonian correction in the waveform (Flanagan & Hinderer 2008) which is much less than our approximation and is independent of the dipolar effect, the tidal deformation does not affect the information of dipole moments in the waveform.

### 5.2. Evaluation of Parameter Estimation

Fisher information matrix (FIM) is employed to characterize the performance in parameter estimation for detectors (Vallisneri 2008). When considering the influence of parameters, the waveform is a



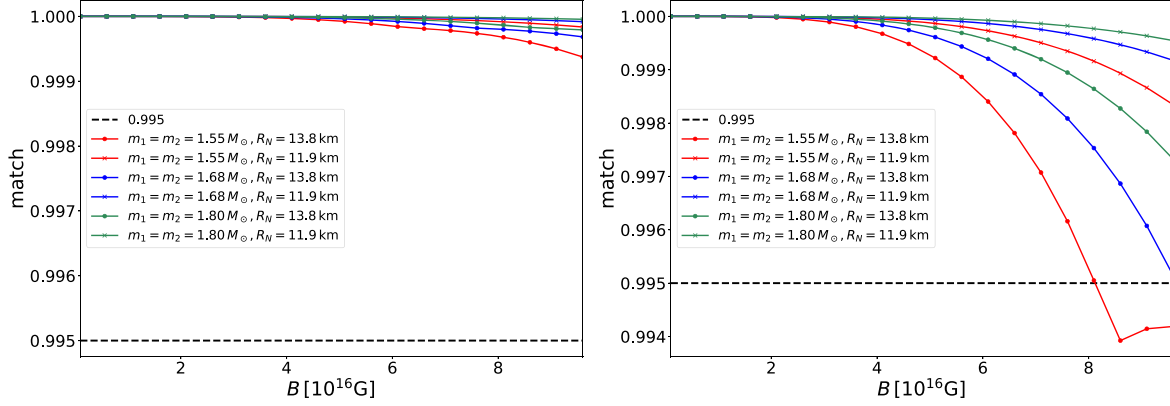


**Figure 3.** For future application of the detection of low-frequency GWs by Taiji and DECIGO, we computed matches between the waveforms with magnetized and non-magnetized neutron stars with different surface magnetic fields using the same parameter set as the former. The left panel shows the values of the match for the DECIGO detector and the right panel is for Taiji.

**Table 1**

Relative Errors of  $d_1$ ,  $D$ ,  $M_c$  are Evaluated using the PSD of both LIGO and ET Detectors, Respectively

	LIGO	ET
$\frac{\Delta d_1}{d_1}$	3.52%	0.26%
$\frac{\Delta D}{D}$	4.31%	0.33%
$\frac{\Delta M_c}{M_c}$	$1.04 \times 10^{-5}$	$3.13 \times 10^{-7}$

**Note.** In the computation, we employ the parameter values of  $m_1 = 1.65 M_\odot$ ,  $m_2 = 1.55 M_\odot$  and  $D = 100$  Mpc. Additionally, we set  $B = 6.0 \times 10^{17}$  G and  $R_N = 13.8$  km so that the magnetic dipole moment is  $d_1 = 7.88 \times 10^{35}$  G · cm<sup>3</sup>.

**Table 2**

Relative Errors of Surface Magnetic Field  $B$  of Different  $m_1$  using the ET Detector

	$m_1 = 1.44 M_\odot$	$m_1 = 1.50 M_\odot$	$m_1 = 1.80 M_\odot$
$\frac{\Delta B}{B}$ for $B = 7.0 \times 10^{14}$ G	24.41%	27.48%	46.93%

**Note.** In the computation, we employ the parameter values of  $m_2 = 1.40 M_\odot$  and  $R_N = 13.8$  km. Note that we set  $D = 20$  kpc for our Milky Way (Goodwin et al. 1998). Choice of Parameters refer to Kalogera & Baym (1996), Cardall et al. (2001).

function of parameters, i.e.,

$$h = h(\lambda_i), \quad (70)$$

where  $\lambda_i$  is the parameter vector with  $i$  ranges from 1 to the total number of parameters. Once we have the waveform Equation (64) we can write the strain amplitude detected by a detector in the frequency domain:

$$h(f) = F_+ h_+ + F_\times h_\times, \quad (71)$$

here the antenna pattern functions  $F_+$  and  $F_\times$  are given by (Maggiore 2007):

$$F_+ = \frac{1}{2}(1 + \cos^2 \theta) \cos 2\phi, \\ F_\times = \cos \theta \sin 2\phi. \quad (72)$$

where  $\theta$  and  $\phi$  denote the sky location. This expression has the same linear combination as that in the time domain because we regard  $\theta$ ,  $\phi$ ,  $\iota$  as time-independent. Thus, the detected strain amplitude relies on the parameters:

$$h = h(f; \lambda_i) = e^{i\Psi_+} \frac{c}{D} \left( \frac{5}{24} \right)^{1/2} \\ \times \left[ \frac{1}{2}(1 + \cos^2 \theta) \cos 2\phi \frac{1 + \cos^2 \iota}{2} \right. \\ \left. + \cos \theta \sin 2\phi \cos \iota e^{i\frac{\pi}{2}} \right] \\ \times \left[ \pi^{-2/3} \left( \frac{GM_c}{c^3} \right)^{5/6} f^{-7/6} - \frac{\pi^{2/3}}{2} c^{-2} \left( \frac{GM_c}{c^3} \right)^{1/6} \right. \\ \left. \times \left( \frac{\mu}{M} \right)^{2/5} \left( \frac{d^2}{24G\mu^2} - \frac{6d_1 d_2}{Gm_1 m_2} \right) f^{1/6} \right] \\ = \frac{1}{4} (1 + \cos^2 \theta) \cos 2\phi (1 + \cos^2 \iota) A e^{i\Psi_+} \\ + \cos \theta \sin 2\phi \cos \iota A e^{i\Psi_\times}, \quad (73)$$

with  $\Psi_\times = \Psi_+ + \pi/2$ .

We are especially interested in the influence of magnetic dipole moments of neutron stars on the waveform. We would like to see how accurately we can estimate and further constrain the parameters through GWs since GWs carry information of the physical properties of neutron stars. Since the surface magnetic fields and radii of neutron stars are completely coupled in magnetic dipole moments, it is advantageous to treat the magnetic dipole moment of the first neutron star as a distinct and independent parameter.

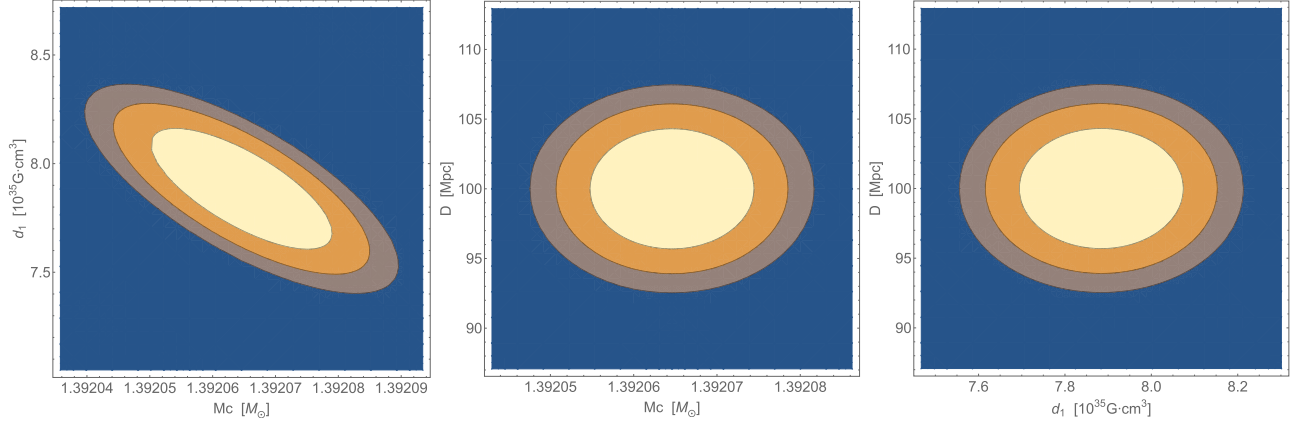


**Figure 4.** Likelihood of parameters derived from FIM. The left-hand panel plotted the likelihood of chirp mass  $M_c$  and the magnetic dipole moment of the first neutron star  $d_1$ . The figure in the middle shows the likelihood of  $M_c$  and the luminosity distance from the binary to our earth  $D$ . The right-hand panel is for  $d_1$  and  $D$ . In the three figures the contours from the outermost to the innermost are  $1\sigma$ ,  $2\sigma$  and  $3\sigma$  levels respectively.

Introducing the FIM for a given waveform  $h$  (Vallisneri 2008):

$$\Gamma_{ij} = \left( \frac{\partial h}{\partial \lambda_i} \middle| \frac{\partial h}{\partial \lambda_j} \right). \quad (74)$$

The square root of the diagonal elements of the inverse of the FIM provides the errors of parameters:

$$\Delta \lambda_i = \sqrt{(\Gamma^{-1})_{ii}}. \quad (75)$$

Then we can calculate the corresponding likelihood:

$$\mathcal{L}(\lambda) \propto e^{-\frac{1}{2} \sum_{i,j} \Gamma_{ij} \Delta \lambda_i \Delta \lambda_j}. \quad (76)$$

For comparison and estimation of the accuracy, we computed relative errors of some main parameters for the two detectors. Note that we regard the magnetic dipole moment of the first neutron star  $d_1$  as the only independent magnetic dipole moment. When calculating the matrix, we set the angles to be  $\theta = \pi/4$ ,  $\phi = \pi/3$ ,  $\iota = \pi/6$  in order to contain  $h_+$ ,  $h_\times$  components. We provide the results for three main parameters in Table 1. Especially, we will show below that it is possible to estimate the magnetic field to a value less than  $10^{16}$  G from the waveform in the Milky Way. It is important to see the lower limit that can be identified. It has been shown that a model can achieve a perfect fit to data for certain parameters when the match satisfies the condition (Chatziioannou et al. 2017):

$$1 - \text{match} < \frac{N}{2\text{SNR}^2} \quad (77)$$

where  $N$  is the number of intrinsic parameters (here  $N = 12$ ) of the waveforms and SNR is the signal-to-noise ratio. On the other hand, this gives the upper limit for a detector to distinguish two waveforms. Instead of a source at distance  $D = 100$  Mpc, we estimated the relative errors for magnetic fields of some BNS systems in our Milky Way. From Table (2) it is shown that in our configuration with surface magnetic field  $B = 7.0 \times 10^{14}$  G

for neutron star  $m_1$ , corresponding to magnetic dipole as  $9.20 \times 10^{32} \text{ G} \cdot \text{cm}^3$ , the relative error can reach within 30%.

The errors derived from the FIM show a promising evaluation in estimating the magnetic dipole moments and chirp mass, due to our selection of an extremely strong magnetic field carried by neutron stars. We plot the contour of the likelihood for LIGO, shown in Figure 4. Note that the method characterizes the performance of a detector in parameter estimation, thus this will give a more optimistic estimation than practice.

## 6. Conclusions and Discussions

The mergers of binary neutron stars are promising electromagnetic counterparts of the GW sources in multi-messenger astronomy. In this paper, we have derived the equation of motion for a binary neutron star system taking into account magnetic dipolar interaction. In our analysis, we calculated the total energy emission rate and the time evolution of orbital radius for circular orbits by using the post-Newtonian method and by considering the lowest order multipole radiation for gravitational and electromagnetic waves. It is shown that both the magnetic dipolar interaction and electromagnetic radiation can modify the orbital motion and evolution. Considering the modification we calculated the gravitational waveform in the frequency domain including terms related to the magnetic dipole moment. It is found that the magnetic dipole moment can introduce a significant phase shift proportional to  $f^{-1/3}$  and introduce an additional term proportional to  $f^{1/6}$  in the amplitude.

After obtaining the waveforms containing magnetic dipole moments, we employ the matched filtering and the FIM for evaluating the parameter estimation for the LVK detectors and future ET detectors. In the strong magnetic field regime, we show that the match of two signals with and without magnetic dipole decreases as the magnetic fields increase. This suggests the

potential for detecting extremely strong magnetic fields or providing constraints on the magnetic fields of neutron stars in future observations by the LVK and ET. The latter could measure or constrain the magnetic field in a higher accuracy. The analysis from FIM provides an optimistic evaluation for the parameter estimations with a high signal-to-noise ratio, especially the estimation of magnetic dipole moments is limited to a few per cent for ET. Furthermore, it is capable to estimate magnetic field at  $\sim 10^{14}$  G to an error within 30% in our Milky Way.

Note that the improved sensitivity of future detectors will result in more detection of GWs from neutron star mergers. Since neutron stars usually carry strong magnetic fields (Duncan & Thompson 1992) which can affect the waveforms, this provides a possibility to detect the strong magnetic fields in future GW observation. Furthermore, we can also give a constraint on the magnitude of magnetic fields and further constrain the equations of the state of neutron stars (Bandyopadhyay et al. 1997; Ferrer et al. 2010). It is important to acknowledge that the spin of a neutron star might not align with its magnetic axis, resulting in a different modification to the dynamics in contrast to the current scenario. Thus in future work we will generalize the current case to the magnetic dipole moments with arbitrary orientation (Weisberg et al. 1981). Further, the modification by magnetic dipole moments introduced in this work can be extended to the black hole-neutron star binaries. Indeed, a rotating black hole in the magnetic fields produced by the neutron star can accrete charges and form a magnetic dipole moment (Wald 1974; Liu et al. 2016), with such effects we can further investigate the black hole-neutron star mergers and give methods to search for charged black holes.

### Acknowledgments

We thank Chen Su for his discussions and suggestions for our coding work. We thank WenBiao Han for his beneficial discussions for this paper. We also thank Belahcene Imene for her valuable advice on this work. This work was supported by the National Key R&D Program of China (grant No. 2021YFC2203002), and the National Natural Science Foundation of China (grant Nos. 12173071 and 12473075). This work made use of the High Performance Computing Resource in the Core Facility for Advanced Research Computing at Shanghai Astronomical Observatory.

### ORCID iDs

Rundong Tang  <https://orcid.org/0000-0002-7282-1612>

### References

- Abadie, J., Abbott, B., Abbott, R., et al. 2010, *CQGra*, **27**, 173001
- Abbott, B., Abbott, R., Abbott, T., et al. 2019, *PhRvX*, **9**, 011001
- Abbott, B., Abbott, R., Abbott, T., et al. 2020, *ApJL*, **892**, L3
- Abbott, B. P., Abbott, R., Abbott, T., et al. 2016a, *PhRvL*, **116**, 131103
- Abbott, B. P., Abbott, R., Abbott, T., et al. 2016b, *PhRvL*, **116**, 061102
- Abbott, B. P., Abbott, R., Abbott, T., et al. 2017, *PhRvL*, **119**, 161101
- Abbott, B. P., Abbott, R., Abbott, T., et al. 2019, *PhRvL*, **123**, 011102
- Abbott, B. P., Abbott, R., Abbott, T. D., et al. 2016c, *ApJL*, **832**, L21
- Abbott, R., Abbott, T., Abraham, S., et al. 2021, *PhRvX*, **11**, 021053
- Acernese, F. a., Agathos, M., Agatsuma, K., et al. 2014, *CQGra*, **32**, 024001
- Anderson, M., Hirschmann, E. W., Lehner, L., et al. 2008, *PhRvL*, **100**, 191101
- Andersson, N., Ferrari, V., Jones, D., et al. 2011, *GReGr*, **43**, 409
- Apostolatos, T. A., Cutler, C., Sussman, G. J., & Thorne, K. S. 1994, *PhRvD*, **49**, 6274
- Baiotti, L. 2019, *PrPNP*, **109**, 103714
- Bandyopadhyay, D., Chakrabarty, S., & Pal, S. 1997, *PhRvL*, **79**, 2176
- Bauswein, A., & Janka, H.-T. 2012, *PhRvL*, **108**, 011101
- Bocquet, M., Bonazzola, S., Gourgoulhon, E., & Novak, J. 1995, *A&A*, **301**, 757
- Bourgoin, A., Le Poncin-Lafitte, C., Mathis, S., & Angonin, M.-C. 2022, *PhRvD*, **105**, 124042
- Cardall, C. Y., Prakash, M., & Lattimer, J. M. 2001, *ApJ*, **554**, 322
- Chatziioannou, K., Klein, A., Yunes, N., & Cornish, N. 2017, *PhRvD*, **95**, 104004
- Christiansen, Ø., Jiménez, J. B., & Mota, D. F. 2021, *CQGra*, **38**, 075017
- Chu, Q., Yu, S., & Lu, Y. 2022, *MNRAS*, **509**, 1557
- Collaboration, T. L. S., & Aasi, J. 2015, *CQGra*, **32**, 074001
- Dall’Osso, S., Stratta, G., Guetta, D., et al. 2011, *A&A*, **526**, A121
- Dietrich, T., Bernuzzi, S., & Tichy, W. 2017, *PhRvD*, **96**, 121501
- Duncan, R. C., & Thompson, C. 1992, *ApJL*, **392**, L9
- Ferrario, L., & Wickramasinghe, D. 2005, *MNRAS*, **356**, 615
- Ferrer, E. J., de la Incera, V., Keith, J. P., Portillo, I., & Springsteen, P. L. 2010, *PhRvC*, **82**, 065802
- Flanagan, E. E., & Hinderer, T. 2008, *PhRvD*, **77**, 021502
- Goldstein, A., Veres, P., Burns, E., et al. 2017, *ApJL*, **848**, L14
- Goodwin, S., Gribbin, J., & Hendry, M. 1998, *Obs*, **118**, 201
- Griffiths, D. J. 2005, *Introduction to Electrodynamics* (Cambridge: Cambridge Univ. Press)
- Griffiths, D. J. 2011, *AmJPh*, **79**, 867
- Henry, Q., Larrouturou, F., & Le Poncin-Lafitte, C. 2024, *PhRvD*, **109**, 084048
- Henry, Q., Larrouturou, F. m. c., & Le Poncin-Lafitte, C. 2023, *PhRvD*, **108**, 024020
- Heras, J. A. 1994, *AmJPh*, **62**, 1109
- Hotokazaka, K., Nakar, E., Gottlieb, O., et al. 2019, *NatAs*, **3**, 940
- Hulse, R. A. 1994, *RvMP*, **66**, 699
- Ioka, K., & Taniguchi, K. 2000, *ApJ*, **537**, 327
- Jackson, J. D. 2021, *Classical Electrodynamics* (New York: Wiley)
- Kalogera, V., & Baym, G. 1996, *ApJ*, **470**, L61
- Landau, L. D., & Lifshitz, E. M. 1975, *The Classical Theory of Fields*. (Oxford: Pergamon)
- Lindblom, L., Owen, B. J., & Brown, D. A. 2008, *PhRvD*, **78**, 124020
- LISA Study Team, K. D., et al. 1997, *CQGra*, **14**, 1399
- Liu, L., Christiansen, Ø., Guo, Z.-K., Cai, R.-G., & Kim, S. P. 2020, *PhRvD*, **102**, 103520
- Liu, T., Romero, G. E., Liu, M.-L., & Li, A. 2016, *ApJ*, **826**, 82
- Luo, Z., Guo, Z., Jin, G., Wu, Y., & Hu, W. 2020, *ResPh*, **16**, 102918
- Maggiore, M. 2007, *Gravitational Waves: Volume 1: Theory and Experiments* (Oxford: Oxford Univ. Press)
- Matsumoto, T., Nakar, E., & Piran, T. 2019, *MNRAS*, **483**, 1247
- Pacini, F. 1967, *Nature*, **216**, 567
- Punturo, M., Abernathy, M., Acernese, F., et al. 2010, *CQGra*, **27**, 194002
- Radice, D., & Dai, L. 2019, *EPJA*, **55**, 1
- Seto, N., Kawamura, S., & Nakamura, T. 2001, *PhRvL*, **87**, 221103
- Somiya, K. 2012, *CQGra*, **29**, 124007
- Spruit, H. C. 2008, *AIP Conf. Proc.: 40 YEARS OF PULSARS: Millisecond Pulsars, Magnetars and More*, 983 (Melville, NY: AIP), 391
- Taylor, J. H. 1994, *RvMP*, **66**, 711
- Vallisneri, M. 2008, *PhRvD*, **77**, 042001
- Vasúth, M., Keresztes, Z., Mihály, A., & Gergely, L. Á. 2003, *PhRvD*, **68**, 124006
- Wald, R. M. 1974, *PhRvD*, **10**, 1680
- Weisberg, J. M., Taylor, J. H., & Fowler, L. A. 1981, *SciAm*, **245**, 74
- Zhang, J., Lyu, Z., Huang, J., et al. 2021, *PhRvL*, **127**, 161101